Journal of JSEM, Vol.11, Special Issue (2011) SS53-SS58

Gas-Liquid Two-Phase Flow through an Orifice in Millimeter-Scale Rectangular Channel

Takashi OKE[1], Takehiko KUMAGAI[2], Olusegun J Ilegbusi[3] and Manabu IGUCHI[2]

[1] Graduate School of Engineering, Hokkaido University, Sapporo 060-8628, Japan
[2] Faculty of Engineering, Hokkaido University, Sapporo 060-8628, Japan
[3] College of Engineering and Computer Science, University of Central Florida, Orlando, FL, USA

(*Received 22 December 2010; received in revised form 8 June 2011; accepted 19 June 2011*)

Abstract
An experimental investigation is carried out on air-water two-phase flow through a plate orifice in a millimeter-scale rectangular channel. The width of the channel is kept constant at 50 mm and the height is varied from 0.19 mm to 2.00 mm. The contraction ratio of the orifice is varied from 0.04 to 0.4, and the thickness of the orifice also is allowed to vary over a wide range. The flow patterns upstream and downstream of the orifice are observed with a high-speed camera and by visual inspection. The conditions for occurrence of the observed flow patterns are presented on a flow pattern map. The velocity of the leading edge of a bubble, representing the bubble velocity, is deduced from the camera images. In the upstream part of the test section the bubble velocity is approximated by the sum of the superficial velocities of air and water. A correlation is proposed for the maximum bubble velocity in the whole test section as a function of the two superficial velocities and the contraction ratio.

Key words
Gas-Liquid Two-Phase Flow, Flow Pattern, Millimeter-Scale System, Rectangular Channel, Orifice

1. Introduction

Gas-liquid two-phase flows are prevalent in a variety of engineering fields such as mechanical, chemical, and atomic power engineering. A typical application uses such flows to enhance heat transfer between liquid and pipe wall. The size of the conventionally used pipes ranges from several centimeters to a few meters. A considerable amount of effort has been devoted to understanding the transport characteristics including flow pattern, pressure drop, and heat transfer [1-6].

Recently, gas-liquid two-phase flows have been extensively used in micro reactors [7], microelectronic devices [8], compact heat exchangers [9, 10], and fuel cells [11, 12]. Although there is a variety of pipe elements such as orifice, abrupt expansion, and abrupt contraction in small scale systems, information on gas-liquid two-phase flows through these pipe elements is quite limited compared to conventional scale pipes. This experimental investigation focuses on flow pattern and bubble velocity in a millimeter-scale rectangular channel. The evaluation of pressure loss and heat transfer in micro channel is of essential importance in practical applications. These quantities can be derived from the data on the volumetric fraction of gas which is closely associated with the bubble velocity. This is one of the reasons why the bubble velocity measurement was carried out in this study.

2. Experimental Apparatus

A schematic diagram of the experimental apparatus is shown in Fig. 1(a). Air and de-ionized water were used as the working fluids. Water was supplied from a reservoir tank into the flow channel by a pump. The flow rate was measured by a flow meter and controlled by the pump equipped with a power inverter. Air was supplied from an air compressor and the flow rate was controlled by a mass flow controller. The water inlet pipe was 5.0 mm in diameter, and the air inlet pipe was mounted concentrically on the water inlet pipe, as shown in Fig.1(b). The superficial velocities of air, j_a, and water, j_w, were calculated using the channel height, h and the channel width, W. The superficial velocity of water was varied up to 0.28 m/s and that of air was varied up to 0.80 m/s. The superficial air velocity was evaluated at a mean pressure between the inlet and outlet of the test section. The flow pattern of air-water two-phase flow passing through the orifice was observed with a high-speed camera at a rate of 1000 fps and by visual inspection.

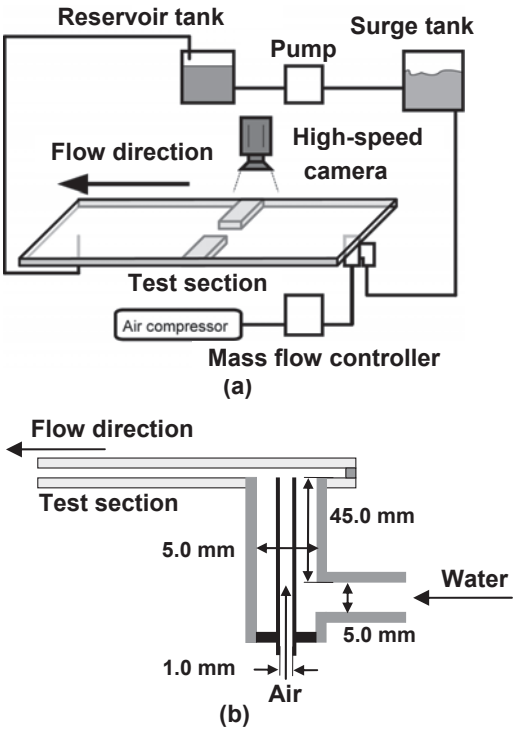

Fig. 1 Schematic diagram of experimental apparatus (a) and the details of air and water inlet (b)

The details of the test section are shown in Fig. 2. The test section was constructed by clipping a thin sheet of fluororesin paper with two transparent glass plates. The

wide face of the test section was placed horizontally. The length of the two glass plates was 465 mm, and the distance between the air and water inlet, and the outlet was 420 mm. The channel width was fixed at W = 50 mm. The orifice was placed 170 mm downstream of the inlet pipe for air and water supply. The channel width at the orifice is denoted by W_o and the thickness of the orifice is L_o.The contraction ratio, β, is defined as the ratio of W_o to W, i.e., $\beta = W_o/W$.

The thicknesses of the thin sheet of paper utilized were 2.00 mm, 1.00 mm, 0.50 mm, and 0.20 mm. The corresponding channel heights were 2.00 mm, 1.00 mm, 0.50 mm, and 0.19 mm, respectively.

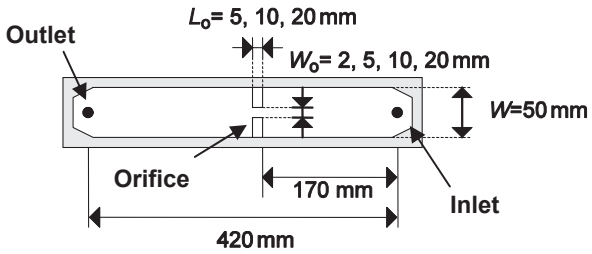

Fig. 2 Details of test section

3. Results and Discussion

3.1 Flow pattern upstream of orifice

The flow patterns of air-water two-phase flow observed in the test section upstream of the orifice can be classified into the following three types, as shown in Fig. 3.

(i) Bubbly flow (denoted by B): Small bubbles move in the continuous liquid phase.

(ii) Slug flow (denoted by S): Large slug-shaped bubbles move in the continuous liquid phase. The length of the bubble is larger than the width of the channel.

(iii) Annular flow (denoted by A): Gas and liquid phases are both in continuous phases. The gas phase exists near the center of the channel.

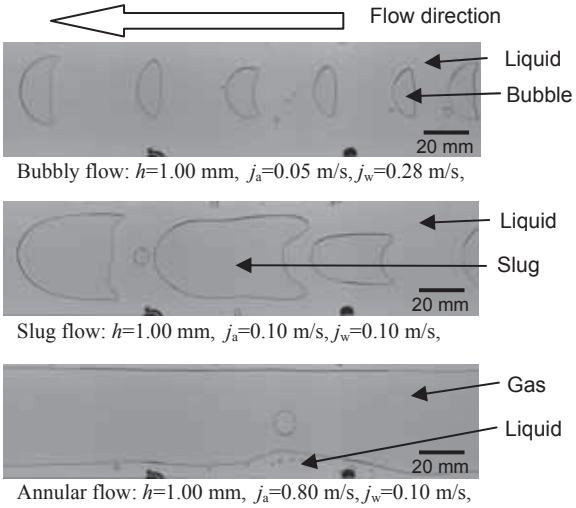

Bubbly flow: h=1.00 mm, j_a=0.05 m/s, j_w=0.28 m/s,

Slug flow: h=1.00 mm, j_a=0.10 m/s, j_w=0.10 m/s,

Annular flow: h=1.00 mm, j_a=0.80 m/s, j_w=0.10 m/s,

Fig. 3 Photographs of basic three flow patterns observed in the test section

3.2 Behavior of air-water two-phase flow just downstream of orifice

The behavior of an air-water two-phase flow just downstream of an orifice can be categorized into the following three types, as shown in Fig. 4.

Type (1): The bubble breaks up into smaller bubbles due to strong shear stress acting on the large bubble during its passage through the orifice.

Type (2): A continuous air cavity appears downstream of the orifice. The trailing bubbles join the cavity and water spreads in the air cavity like a water spray jet.

Type (3): Bubbles passing through the orifice are squeezed and then elongated. There is no bubble breakup into smaller bubbles.

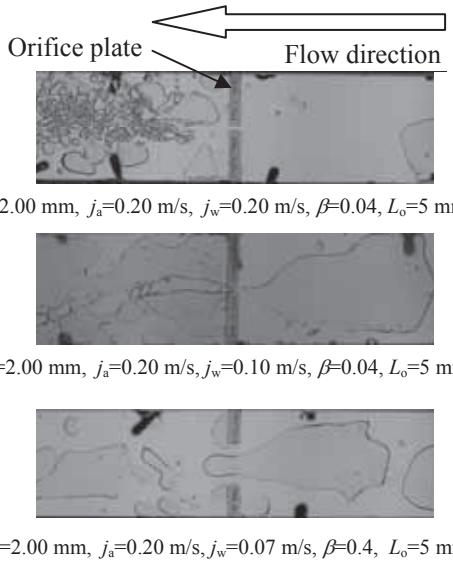

Type (1): h=2.00 mm, j_a=0.20 m/s, j_w=0.20 m/s, β=0.04, L_o=5 mm

Type (2): h=2.00 mm, j_a=0.20 m/s, j_w=0.10 m/s, β=0.04, L_o=5 mm

Type (3) : h=2.00 mm, j_a=0.20 m/s, j_w=0.07 m/s, β=0.4, L_o=5 mm

Fig. 4 Photographs of observed flow patterns (The black spots seen in the photograph are the shade of the attachment behind the test section.)

3.3 Effect of channel height on flow pattern upstream and just downstream of orifice

The maps of the flow pattern for channel heights h=2.00, 1.00, 0.50, and 0.19 mm are shown in Figs. 5 through 8. The contraction ratio, β, and orifice thickness, L_o, were fixed at 0.04 and 5 mm, respectively. The ordinate of each figure is the superficial velocity of air, j_a, and the abscissa is that of water, j_w. The pressure in the test section was increased above the atmospheric pressure especially for h=0.19 mm.

The bubbly, slug, and annular flows, which denoted by B, S, and A, respectively are observed in the test section upstream of the orifice. The upper solid line denotes the boundary between A and S, while the lower one indicates that between S and B. Figures 5 to 8 indicated that the flow patterns for the conditions investigated in this study consist mainly of bubbly and slug flows. Annular flow is observed only in the region of high superficial velocity of air and low superficial velocity of water in Figs. 5 to 7. The boundary between the slug and annular flows and that between the bubbly and slug flows shifts in the higher

superficial air velocity region as the channel height decreases.

The flow patterns downstream of the orifice are denoted by three symbols (△,○,□) in Figs. 5 through 13. That is, Type (1) is denoted by the symbol △, Type (2) by ○, and Type (3) by □. The transition area from Type (1) to Type (2) is denoted by a solid circle (●). Precise measurement was not carried out for j_w= 0.1 m/s in Fig. 8 because the experimental accuracy for water flow rate was not satisfactory. In Figs. 5 through 7, Type (2) is observed in the low j_w region, while Type (1) is common in the remaining region. Type (1), the typical flow pattern in conventional-scale pipes and ducts, disappears completely in the channel with h=0.19 mm, as seen in Fig. 8, while Type (3) appeared at the first time in this figure. Consequently, the effects of volumetric forces on the flow pattern becomes very small compared to those of the surface force under this condition.

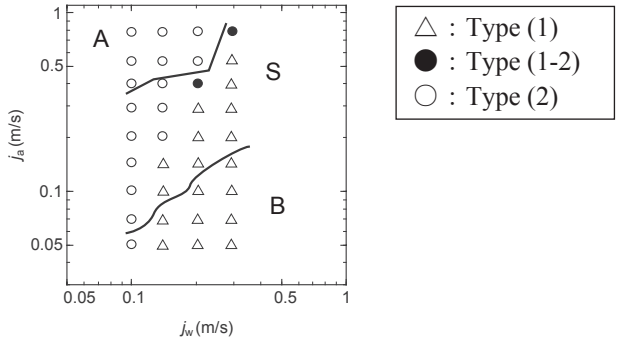

Fig. 5 Flow pattern map for h=2.00 mm, β=0.04, and L_o=5 mm

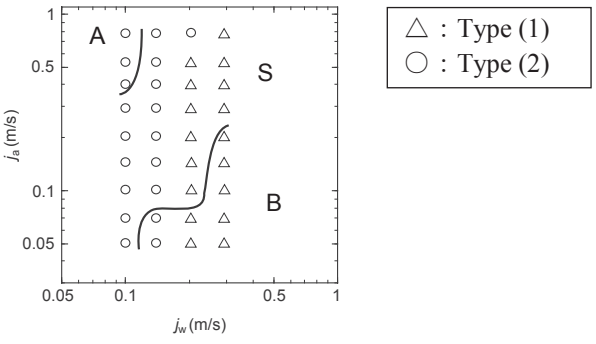

Fig. 6 Flow pattern map for h=1.00 mm, β=0.04, and L_o=5 mm

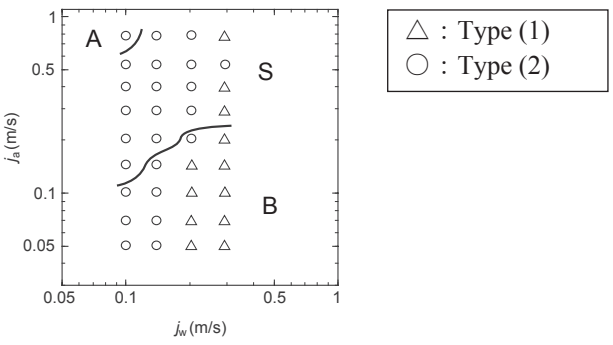

Fig. 7 Flow pattern map for h=0.50 mm, β=0.04, and L_o=5 mm

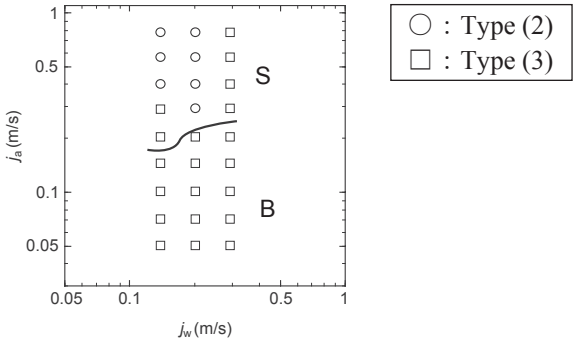

Fig. 8 Flow pattern map for h=0.19 mm, β=0.04, and L_o=5 mm

3.4 Effect of contraction ratio on flow pattern upstream and just downstream of orifice

The flow pattern maps for β=0.04, 0.1, 0.2, and 0.4 are shown in Figs. 5, 9, 10, and 11, respectively. The channel height and the orifice thickness were fixed at h=2.00 mm and L_o=5 mm, respectively. The flow pattern upstream of the orifice is not significantly affected by the contraction ratio under the present experimental conditions. In Figs. 5, 9, and 10, Type (1) and Type (2) patterns are observed in the low j_w region. On the other hand, Type (3) is observed for β = 0.4 in Fig.11. This is because the shear stress is not sufficient to tear off the bubble in the orifice with large contraction ratio. Consequently, the surface force becomes dominant with an increase in β.

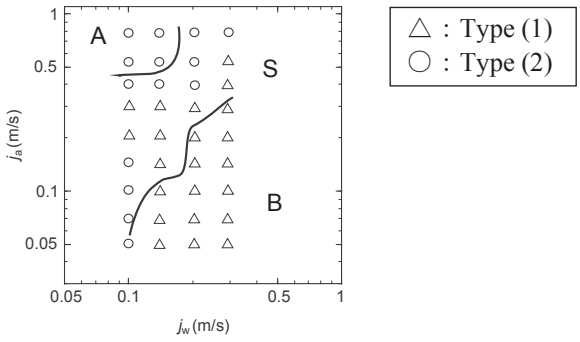

Fig. 9 Flow pattern map for h=2.00 mm, β=0.1, and L_o=5 mm

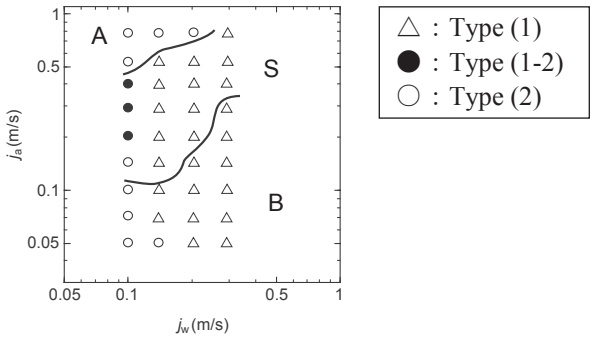

Fig. 10 Flow pattern map for h=2.00 mm, β=0.2, and L_o=5 mm

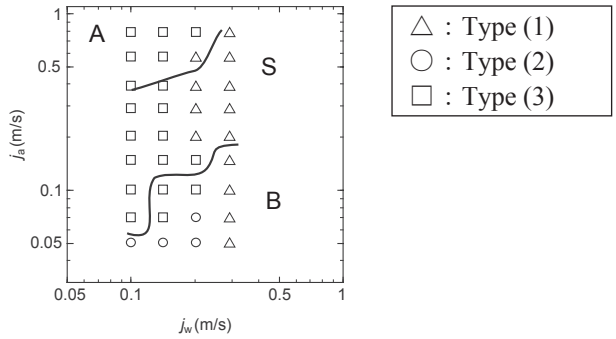

Fig. 11 Flow pattern map for h=2.00 mm, β=0.4, and L_o=5 mm

3.5 Effect of orifice thickness on flow pattern upstream and just downstream of orifice

The flow pattern maps for L_o=5, 10 and 20 mm are shown in Figs. 5, 12, and 13, respectively. The channel height and the contraction ratio were fixed at h=2.00 mm and β = 0.04, respectively.

As shown in Figs. 5 and 12, the flow patterns upstream and downstream of the orifice are not significantly affected by a change in the orifice thickness. Type (3) flow pattern is observed in Fig. 13, implying that the surface force prevails as the orifice thickness increases.

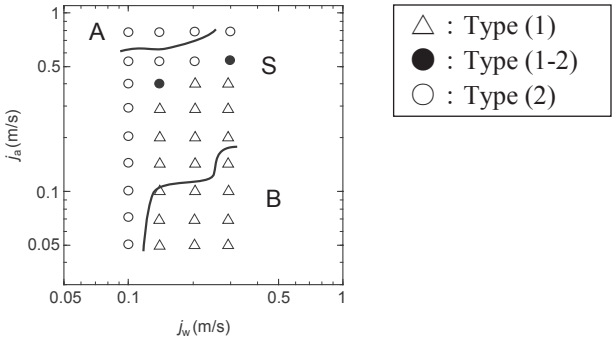

Fig. 12 Flow pattern map for h=2.00 mm, β=0.04, and L_o=10 mm

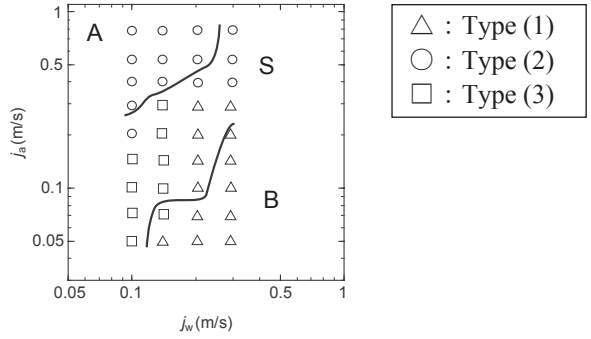

Fig. 13 Flow pattern map for h=2.00 mm, β=0.04, and L_o=20 mm

3.6 Velocity of bubble passing through orifice

The velocity of the leading edge of a bubble passing through an orifice was measured from the photographs taken by a high-speed camera at 1000 fps. This velocity, used to represent the bubble velocity, u_B, was calculated from the axial displacement of the bubble for every 1/100 second. The relationship between the total superficial velocity, j_T (= j_a +j_w), and the measured bubble velocity in the test section upstream of the orifice, $u_{B,up}$, is shown in Fig. 14. The $u_{B,up}$ value is a mean of the bubble velocities in the test section more than 15mm upstream of the orifice. The bubble velocity, $u_{B,up}$, is adequately approximated by the following relation applicable in conventional scale horizontal pipes and channels:

$$u_{B,up} = j_T = j_a + j_w \quad (1)$$

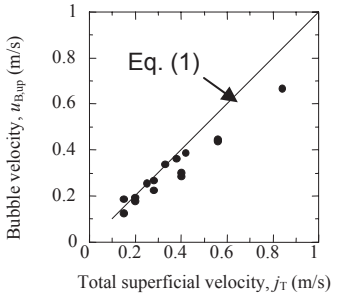

Fig. 14 Relationship between bubble velocity and the total superficial velocity

The measured values of bubble velocity, u_B, for different four contraction ratios in a rectangular channel of h = 2.00 mm are shown in Fig. 15. The thickness of the orifice, L_o, was kept constant at 5 mm. The maximum bubble velocity is observed near the entrance of the orifice and increases with a decrease in the contraction ratio, β. Figures 16 and 17 present the bubble velocity data for different channel heights and orifice thicknesses. The maximum velocity also occurs near the entrance of the orifice under all experimental conditions investigated in this study.

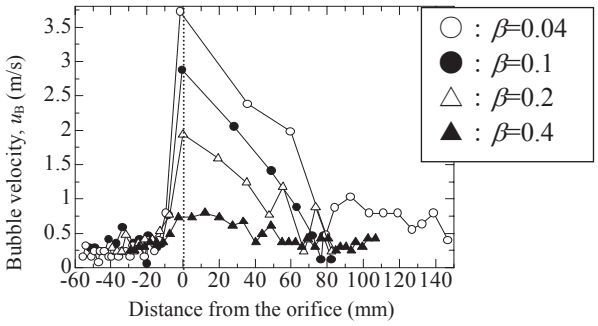

Fig. 15 Bubble velocity for four contraction ratios (h=2.00 mm, L_o=5 mm, j_a=0.14 m/s, and j_w=0.14 m/s)

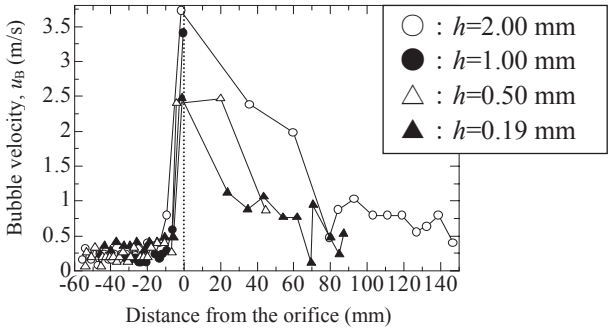

Fig. 16 Bubble velocity for four channel heights (β=0.04, L_o=5 mm, j_a=0.14 m/s, and j_w=0.14 m/s)

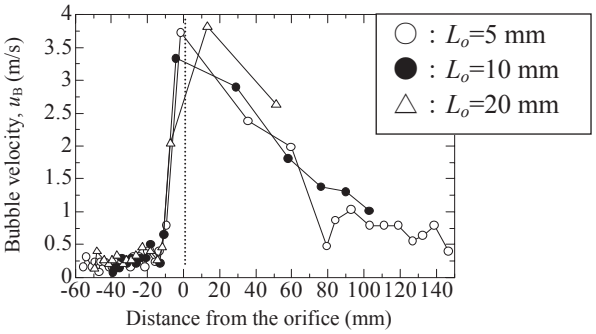

Fig. 17 Bubble velocity for three orifice thicknesses (h=2.00 mm, β=0.04, j_a=0.14 m/s, and j_w=0.14 m/s)

Figure 16 shows that the maximum bubble velocity decreases as the channel height decreases. This is because the bubble is strongly constricted by the channel wall in the case of small channel height. In the 1.0 mm height channel, bubble coalescence took place and, hence, the bubble velocity was not measured. The effect of the orifice thickness, L_0, on the bubble velocity is negligibly small, as seen in Fig. 17.

The measured values of the maximum bubble velocity, $u_{B,max}$, is compared in Fig. 18 with the following relation:

$$u_{B,max} = j_T / \beta \quad (2)$$

The measured values in the low j_T/β regime (j_T/β<6 m/s) is adequately approximated by Eq.(2). On the other hand, $u_{B,max}$, decreases and deviates significantly from Eq.(2) in the high j_T/β regime (j_T/β>6 m/s).

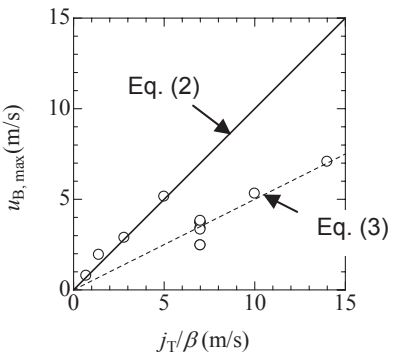

Fig. 18 Relationship between maximum bubble velocity, $u_{B,max}$, and j_T/β

The discrepancy in the high j_T/β regime is attributed to the change in the flow pattern. In the high j_T/β regime, most of the flow patterns are classified into the slug flow regime. In this regime, the gas and liquid phases flow separately near the orifice. This is the reason for the observed decrease in the value of $u_{B,max}$ and its deviation from Eq.(2). The measured values of $u_{B,max}$ in the higher j_T/β regime can be approximated by the following relation:

$$u_{B,max} = 0.50 j_T / \beta \quad (3)$$

As depicted in the introduction, information on void fraction is of essential importance for correlating the pressure loss of gas-liquid two-phase flows and heat transfer characteristics in micro channels. If bubbles are dispersed uniformly in a pipe and move downstream at the same velocity everywhere in the pipe without deformation, breakup, and coalescence, the void fraction can be obtained from j_g/u_B, where j_g is the superficial velocity of gas and, u_B, is the bubble velocity. However, bubbles observed in this study are not uniformly dispersed in the pipe and are subjected to deformation and so on. The bubble velocity, u_B, therefore was determined only focusing on the motion of the leading edge of a bubble. Accurate evaluation of the void fraction may become possible by collecting more detailed data on bubble size and velocity.

4. Conclusions

The effects of an orifice on the flow pattern and bubble velocity in gas-liquid two-phase flows in millimeter-scale rectangular channels were experimentally investigated. The bubbly, slug, and annular flows were observed in the test section upstream of the orifice. The major findings of this study can be summarized as follows.

1. The flow patterns observed just downstream of the orifice are classified into the following three types.

   Type (1): A bubble breaks up into many smaller bubbles due to strong shear stress acting on the bubble during its passage through the orifice.

   Type (2): A continuous air cavity appears downstream of the orifice. The trailing bubbles join the cavity and water spreads in the air cavity.

   Type (3): Bubbles passing through the orifice are squeezed and elongated. There is no break up of bubble into smaller bubbles.

2. The surface force becomes dominant with a decrease in the channel height, h, an increase in the contraction ratio, β, and an increase in the orifice thickness, L_o.
3. The bubble velocity upstream of the orifice, $u_{B,up}$, is nearly equal to the total superficial velocity of gas and liquid, j_T. The maximum bubble velocity, $u_{B,max}$, is approximated by Eq.(2) in the low j_T/β regime. In the high j_T/β regime, $u_{B,max}$, is approximated by Eq.(3).

Nomenclature

h channel height, mm
j superficial velocity, m/s
L_o orifice thickness, mm
u_B bubble velocity, m/s
β contraction ratio (= W_o/W), -

Subscripts

w water
a air
o orifice
T total

References

[1] Taitel, Y. and Dukler, E., A.: A Model for Predicting Flow Regime Transitions in Horizontal and Near Horizontal Gas-Liquid Flow, *Int. AIChE J.*, **22**-1(1976), 47-54 .

[2] Triplett, A., K., Ghiaasiaan, M., S., Abdel-Khalik, I., S. and Sadowaki, L., D.: Gas-Liquid Two-Phase Flow in Microchannels, Part I: Two-Phase Flow Patterns, *Int. J. Multiphase Flow*, **25** (1999), 377-394.

[3] Lockhart, W., R. and Martinelli, C., R.: Proposed Correlation of Data for Isothermal Two-Phase, Two-Component Flow in Pipes, *Chemical Engineering Progress*, **45**-1(1949), 39-48.

[4] Chisholm, D.: A Theoretical Basis for the Lockhart-Martinelli Correlation for Two-Phase Flow, *Int. J. Heat and Mass Transfer*, **10**(1967), 1767-1778.

[5] Maeda, D. and Iguchi, M.: Attachment of an Annular Bubble to an Orifice Placed in Gas-Liquid Flow (in Japanese), *Tetsu-to-Hagane*, **92** (2006), 34-36.

[6] Davidson, L. and Amick, H., E., JR.: Formation of Gas Bubbles at Horizontal Orifices, *A.I.Ch.E. J.*, **2-3** (1956), 337-342.

[7] Reyes, R., D., Iossifidis, D., Auroux, P.-A. and Manz, A.: Micro Total Analysis Systems. 1. Introduction, Theory, and Technology, *Anal. Chem.*, **74**-12(2002), 2623-2636.

[8] Naphon, P. and Wiriyasart, S.: Liquid Cooling in the Mini-Rectangular Fin Heat Sink with and without Thermoelectric for CPU, *Int. Com. Heat and Mass Transfer,* **36** (2009), 166-171.

[9] Asano, H., Takenaka, N. and Fujii., T.: Flow Characteristics of Gas-Liquid Two-Phase Flow in Plate Heat Exchanger (Visualization and Void Fraction Measurement by Neutron Radiography), *Exp Thermal and Fluid Science*, **28**(2004), 223-230.

[10] Takeuchi, Y., Park, C., Noborio, K., Yamamoto, Y. and Konishi, S.: Heat Transfer in SiC Compact Heat Exchanger, *Fusion Engineering and Design*, in press.

[11] Bewer, T., Beckmann, T., Dohle, H., Mergel, J. and Stolten, D.: Novel Method for Investigation of Two-Phase Flow in Liquid Feed Direct Methanol Fuel Cells Using an Aqueouos H_2O_2 Solution, *Journal of Power Sources*, **125** (2004),1-9.

[12] Choban, R., E., Markoski, J., L., Wieckowski, A. and Kenis, J., A., P.: Microfluidic Fuel Cell Based on Laminar Flow, *Journal of Power Sources*, **128** (2004), 54-60.